Preparation, Crystal and Magnetic Structure of the Double Perovskites Ba_2CoBO_6 (B = Mo, W)

María J. Martínez-Lope,[a] José A. Alonso,*[a] María T. Casais,[a] and María T. Fernández-Díaz[b]

Keywords: Perovskite structure / Neutron diffraction / Magnetic properties / Antiferromagnetic ordering / Cobalt

Ba_2CoBO_6 (B = Mo, W) perovskites have been prepared in polycrystalline form by thermal treatment, in air, of previously decomposed citrate precursors. These materials have been characterized by X-ray (XRD) and neutron powder diffraction (NPD) data and magnetization measurements. At room temperature, the crystal structure is cubic, space group $Fm\bar{3}m$, with a = 8.08623(3) and 8.10799(3) Å for the Mo and W compounds, respectively. The crystal contains alternating CoO_6 and $Mo(W)O_6$ octahedra, with an almost negligible anti-site disordering. The low temperature antiferromagnetic ordering has been followed from sequential neutron diffraction data. Peaks of magnetic origin appear at the NPD patterns below temperatures of T_N = 27 K and T_N = 19 K for the Mo and W compounds, respectively. The magnetic structures are both defined by a propagation vector k = (1/2, 1/2, 1/2). They can be described as an array of ferromagnetic layers of Co moments, perpendicular to the [111] directions, coupled antiferromagnetically. The refined magnitude of the Co^{2+} magnetic moments suggests a high-spin electronic configuration (S = 3/2); covalence effects account for the slight reduction in the low-temperature ordered moments, although this effect is minimized for the W compound. Structural and magnetic features are discussed in relation to the chemical nature of the species present in the solids.

Introduction

The description of colossal magnetoresistance (CMR) properties in perovskite-related materials has triggered a revival of interest in transition metal oxides in an effort to optimize the observed CMR properties and to understand the involved mechanisms. CMR materials undergo a large change in electrical resistance in response to an external magnetic field. In these compounds, the applied field tends to align the local spins and hence leads to a rapid drop of the measured resistivity by suppressing spin fluctuations and enhancing electronic transfer. CMR was first reported in $LaMnO_3$ perovskite derivatives; further research demonstrated that it is also present in a range of compounds, most of them exhibiting ferromagnetic and semimetallic characteristics simultaneously.[1,2] It is well established now that the ferromagnetic Curie temperature of mixed-valence manganites (based upon $LaMnO_3$) cannot be increased above 400 K by any chemical substitution. Materials with a substantially higher T_c must be developed to operate in a useful temperature range around room temperature.

Recently, the double perovskite Sr_2FeMoO_6 has been proposed as a half-metallic ferromagnet and an alternative to perovskite manganites.[3−7] Further studies on other double perovskites seem to indicate that the occurrence of MR properties is a common feature in some of them. The A = Ca, Ba analogues of the A_2FeMoO_6 family were also found to exhibit semimetallic and ferromagnetic properties.[8,9] Furthermore, Sr_2FeReO_6 has[10] an electronic structure similar to that of Sr_2FeMoO_6: these results have expanded the options for optimizing CMR properties for specific technological applications, searching in other members of the wide family of perovskites of composition $A_2B'B''O_6$ (A: alkaline earth metal; B′, B″: transition metals).

We have become interested in revisiting other transition metal double perovskites, prepared in the Sixties and forgotten for more than 30 years. We have chosen the Co derivatives in the series A_2CoBO_6 (A = Ba, Sr; B = Mo, W). Recently, we described CMR properties in conveniently reduced $Sr_2CoMoO_{6-\delta}$;[11] we have now focused our attention on the Ba derivatives. There is very little literature concerning these phases. Ba_2CoBO_6 (B = Mo, W) perovskites were first studied in the sixties.[12−15] The crystal structure of the Mo phase was described as cubic (with a = 4.043 Å) assuming a random distribution of Co and Mo cations. The W compound was also reported to be cubic, with a = 8.098 Å, exhibiting an ordered $(NH_4)_3FeF_6$ crystal structure. There are a few studies on their magnetic properties;[16−18] Ba_2CoWO_6 was reported to be an antiferromagnet with T_N = 17 K.[16] Its magnetic structure was also studied by

[a] Instituto de Ciencia de Materiales de Madrid, C.S.I.C., Cantoblanco, 28049 Madrid, Spain
[b] Institut Laue-Langevin, B. P. 156, 38042 Grenoble Cedex 9, France

neutron diffraction at 4.2 K,[19] and described as ferromagnetic [111] Co layers coupled antiparallel to adjacent Co layers. There are no reports on the magnetic structure of the Mo compound.

In the present work we describe the synthesis of Ba_2CoBO_6 (B = Mo, W), prepared by soft chemistry procedures, and the results of a neutron diffraction (NPD) study on well-crystallized samples. The crystal structure has been revisited; we report complete structural data for these perovskites. The magnetic data suggest the presence of an unquenched orbital contribution to the effective magnetic moment. Low temperature NPD data allowed us to probe the microscopic origin of the antiferromagnetic ordering, and the evolution of the ordered Co^{2+} magnetic moments.

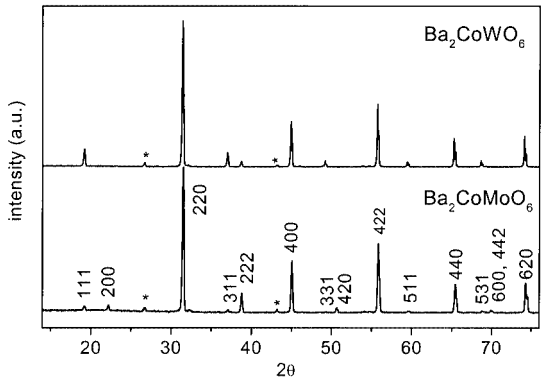

Figure 1. XRD patterns for Ba_2CoBO_6 (B = Mo, W), indexed in a cubic unit cell with $a = 2a_0$, $a_0 \approx 4$ Å; the asterisks indicate the main reflections of the $BaBO_4$ impurity phases

Results

The perovskites Ba_2CoBO_6 (B = Mo, W) were obtained as well crystallized powders; the XRD diagrams are shown in Figure 1. The patterns are characteristic of perovskite structures, showing superstructure peaks (with odd indices) corresponding to the Co/B (B = Mo, W) ordering. The superstructure peaks are more intense in the W compound, due to the higher difference in scattering power with respect to Co. Minor amounts of $BaBO_4$ (B = Mo, W) were detected from both XRD and NPD data; the main reflections of the impurities are indicated with a star in Figure 1.

Magnetic Data

The magnetic susceptibility vs. temperature data for Ba_2CoBO_6 (B = Mo, W) are displayed in Figure 2. The susceptibility exhibits, in both cases, a low temperature maximum, at $T_N = 20$ K and 17 K for B = Mo, W, respectively.

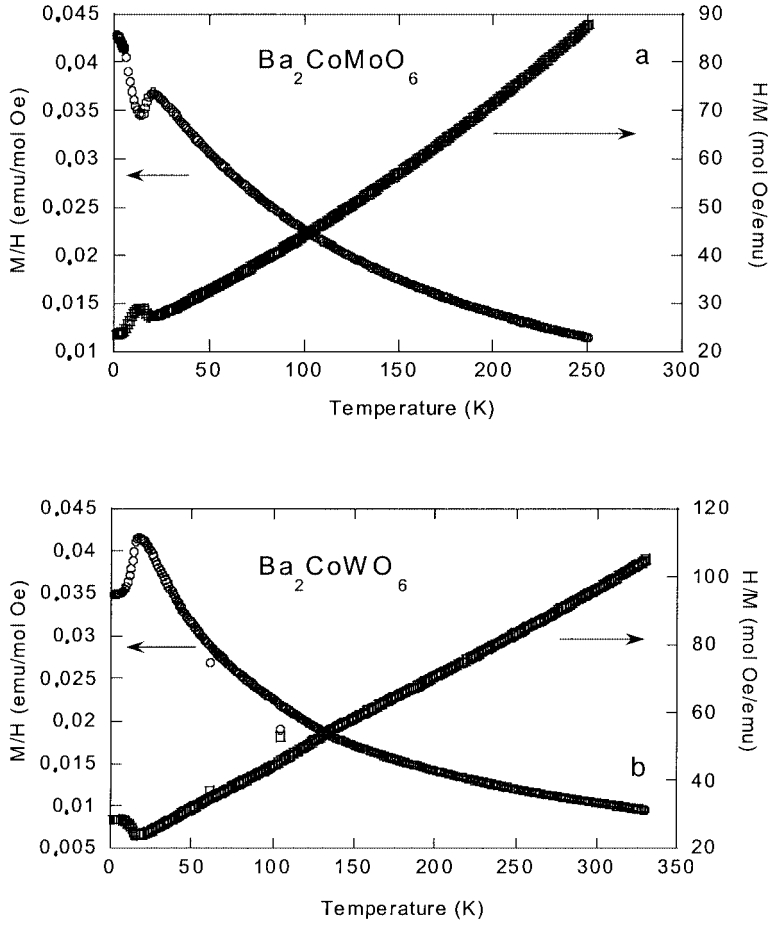

Figure 2. Thermal evolution of the magnetic susceptibility (left axes) and the reciprocal susceptibility (right axes) for (a) Ba_2CoMoO_6 and (b) Ba_2CoWO_6

These maxima correspond to the transition from the high-temperature paramagnetic state to a low-temperature antiferromagnetically ordered phase. A similar Néel temperature (17 K) has been reported for the B = W compound.[17] The reciprocal susceptibility data above T_N (right axes of Figure 2) show a slight curvature, probably due to crystal field effects or a progressive change in the population of the low-spin vs. high-spin electronic configurations for Co cations. A tentative Curie−Weiss fit above 100 K gives paramagnetic moments of 5.24 μ_B/f.u. (f.u. = formula unit) and 5.58 μ_B/f.u. for B = Mo and W, respectively. These values are much larger than expected for spin only Co^{2+}/Mo^{6+} (in any spin configuration for Co^{2+}). This point will be discussed in detail later. The Weiss temperatures of −47.1 K and −75.2 K for B = Mo, W, respectively, confirm the presence of antiferromagnetic interactions in the paramagnetic region. The magnetization vs. field data displayed in Figure 3 are also characteristic of antiferromagnetically ordered systems. The field evolution of the magnetization at 5 K is perfectly linear, excluding the presence of any weak ferromagnetic effect.

Structural Refinement

The structural refinement from room temp. high resolution NPD data was performed in the $Fm\bar{3}m$ space group (No. 225), $Z = 4$, with unit-cell parameters related to a_0 (ideal cubic perovskite, $a_0 \approx 4$ Å) as $a = b = c = 2a_0$. The Ba atoms were located at *8c* positions, Co at *4a*, Mo or W at *4b* sites, and oxygen atoms at *24e* positions. Minor impurities of $BaBO_4$ (B = Mo, W) were included in the refinement as second phases, defined in the space group $I4_1/a$. From the scale factors, the amount of impurity phase is 4.5% and 5.2% for Mo and W, respectively. An excellent fit was obtained for this model, as shown in Figure 4. In the final refinement, the possibility of anti-site disordering was checked by assuming that some Co atoms could occupy Mo or W sites, and vice versa: the refinement of the inversion degree led to less than 1% of anti-site disordering. The oxygen stoichiometry was also checked by refining its occupancy factors; no deficiency was detected within the standard deviations. The most important structural parameters of the crystallographic

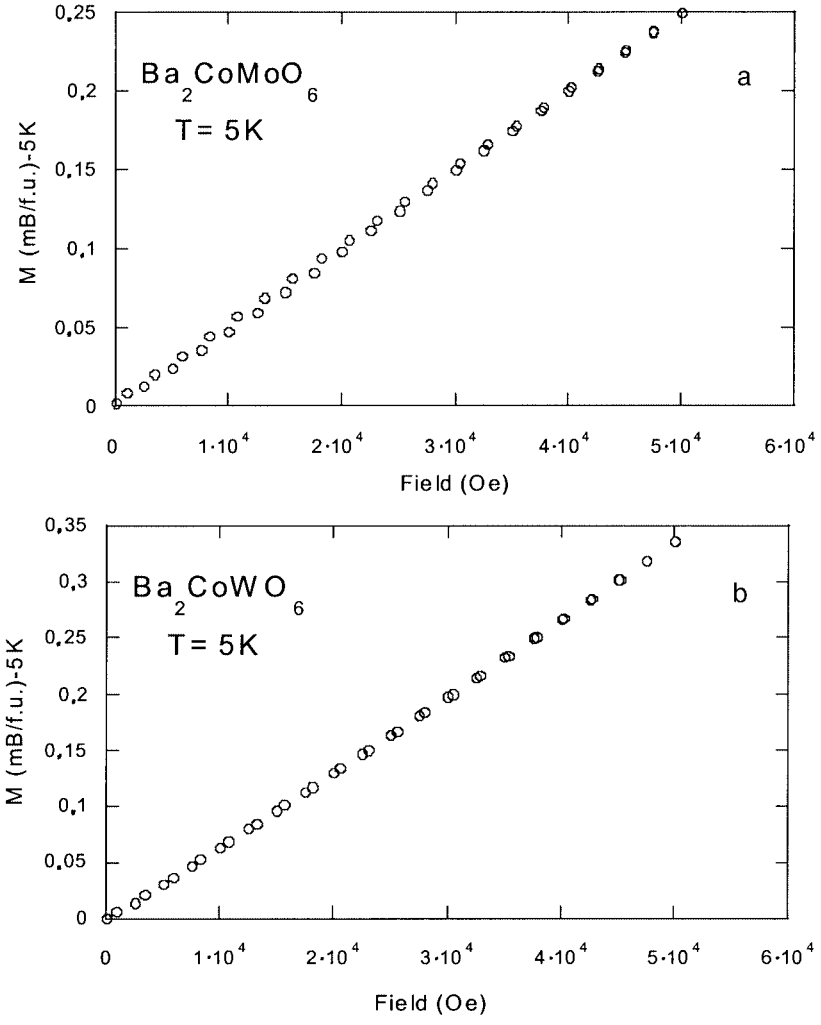

Figure 3. Magnetization vs. field plots for (a) Ba_2CoMoO_6 and (b) Ba_2CoWO_6

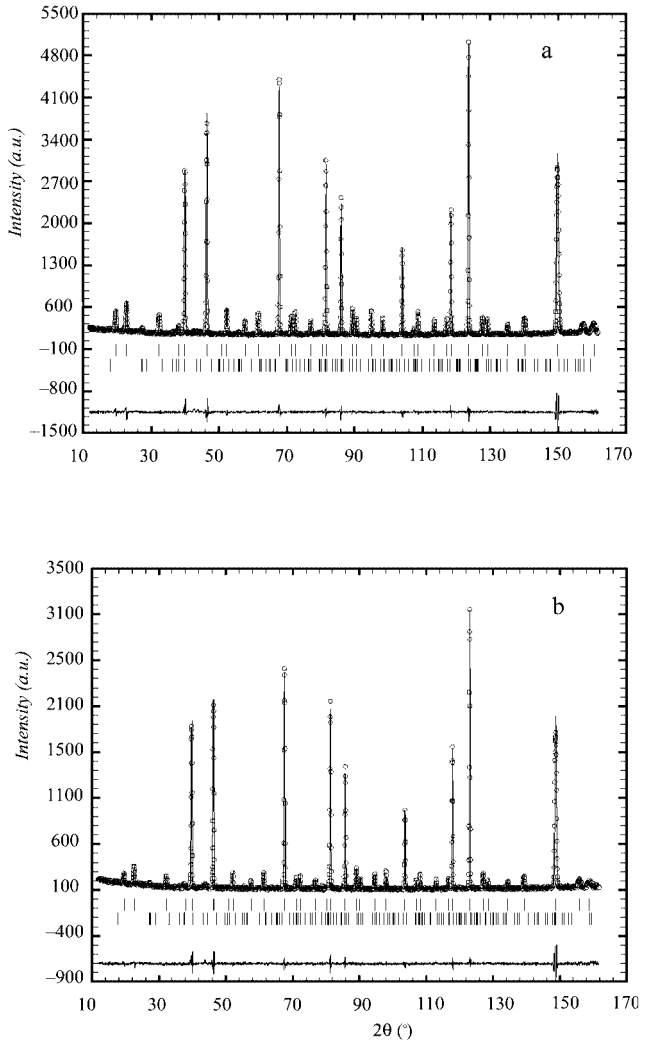

Figure 4. Observed (crosses), calculated (full line) and difference (bottom) high resolution NPD Rietveld profiles for Ba_2CoBO_6 at 295 K for (a) B = Mo, (b) B = W; the second series of tick marks correspond to the Bragg reflections of the $BaBO_4$ impurity phase

structure at room temp. and the discrepancy factors after the refinements are listed in Table 1. The main interatomic distances and angles are included in Table 2. A view of the crystal structure is shown in Figure 5.

The cubic unit cell of Ba_2CoWO_6 is slightly larger than that of Ba_2CoMoO_6, as expected for the larger ionic radius of W^{6+} (0.60 Å) versus Mo^{6+} (0.59 Å) in octahedral coordination.[20] It is interesting to note the significant expansion of the Co−O interatomic distances (Table 2) from the Mo compound [Co−O: 2.114(1) Å] to the W perovskite [Co−O: 2.129(1) Å]. This expansion of Co−O bond lengths is a result of the competing interactions of Co−O and B−O (B = Mo, W) bonds through common oxygens; the higher electronegativity of W than Mo accounts for a more covalent (or less ionic) W−O bond and a weakening of the Co−O chemical bonding in Ba_2CoWO_6.

Magnetic Structure

The magnetic structure of Ba_2CoMoO_6 and its thermal evolution was analyzed by considering a set of NPD patterns collected in the range $2 < T < 72$ K with $\lambda = 2.42$ Å. On decreasing the temperature below 27 K, new reflections appear at positions forbidden for the Bragg reflections in the space group $Fm\bar{3}m$. These new peaks correspond to magnetic satellites defined by the propagation vector $k = (1/2, 1/2, 1/2)$. An antiferromagnetic structure was modeled with magnetic moments at the Co positions; after the full refinement of the profile, including the magnetic moment

Table 1. Unit cell, positional and thermal parameters for Ba_2CoBO_6 (B = Mo, W) in the cubic $Fm\bar{3}m$ space group, from NPD data at 295 K

	B = Mo	B = W
$a = b = c$ (Å)	8.08623(3)	8.10799(3)
V (Å^3)	528.734(3)	533.015(4)
Ba *8c* (1/4, 1/4, 1/4)		
B (Å^2)	0.40(2)	0.37(2)
Co *4a* (0, 0, 0)		
B (Å^2)	0.68(7)	0.54(8)
B *4b* (1/2, 0, 0)		
B (Å^2)	0.24(2)	0.22(4)
O *24e* (x, 0, 0)		
x	0.2614(1)	0.2625(1)
B (Å^2)	0.59(1)	0.52(1)
Reliability factors		
R_p (%)	4.26	4.54
R_{wp} (%)	5.76	6.03
R_{exp} (%)	3.69	4.41
χ^2	2.43	1.87
R_I (%)	2.08	2.04

Table 2. Main bond lengths (Å) and selected angles (°) for cubic Ba_2CoBO_6 (B = Mo, W) determined from NPD data at 295 K

	B = Mo	B = W
Ba−O1 (×12)	2.8604(7)	2.8684(6)
Co−O1 (×6)	2.114(1)	2.1288(8)
B−O1 (×6)	1.930(1)	1.9252(8)
Co−O1−B	180.0	180.0
O1−Co−O1	90.0	90.0
O1−B−O1	90.0	90.0

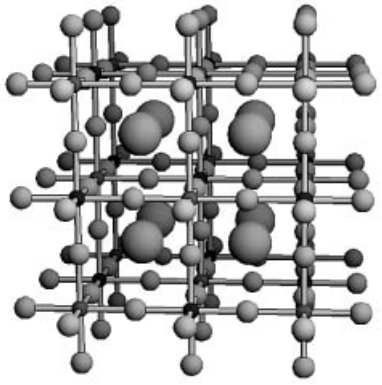

Figure 5. A view of the crystal structure of the Ba_2CoMoO_6 double perovskite; each CoO_6 octahedron is linked to six MoO_6 octahedra

magnitude, a discrepancy factor R_{mag} of 10.6% was reached for the 2 K diagram, collected with a longer counting time. The determination of the orientation of the moments is not possible in a cubic structure from powder data. We supposed that the moments are lying along the [001] direction. The magnetic structure is stable from 2 K to T_N, as demonstrated in a sequential refinement in all the available temperature range. The thermal evolution of the magnetic moments at the Co positions and the lattice parameter are shown in Figure 6 and 7. The good agreement between the observed and calculated pattern at $T = 2$ K is illustrated in Figure 8a. For Ba_2CoWoO_6, the magnetic reflections appear at temperatures below $T_N = 19$ K; these reflections can be indexed with the same propagation vector $k = (1/2, 1/2, 1/2)$. After the refinement of the antiferromagnetic structure, a discrepancy factor of $R_{mag} = 13.6\%$ was obtained. The evolution of the magnetic moments and a unit-cell parameter with temperature are displayed in Figure 6b and 7b; the goodness of the fit at 2 K, including the magnetic structure, is depicted in Figure 8b. A view of the magnetic structure for both materials is shown in Figure 9. It consists of ferromagnetic layers of Co moments, perpendicular to the [111] directions, coupled antiferromagnetically. This magnetic structure compares well with that determined by Cox et al. for Ba_2CoWO_6.[19]

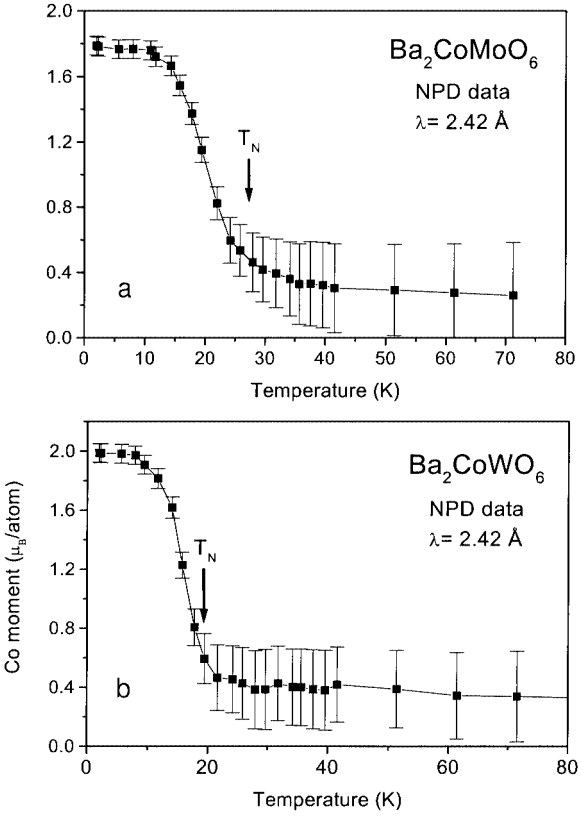

Figure 6. Thermal variation of the ordered Co magnetic moment for the antiferromagnetic structure of Ba_2CoBO_6: (a) B = Mo (b) B = W

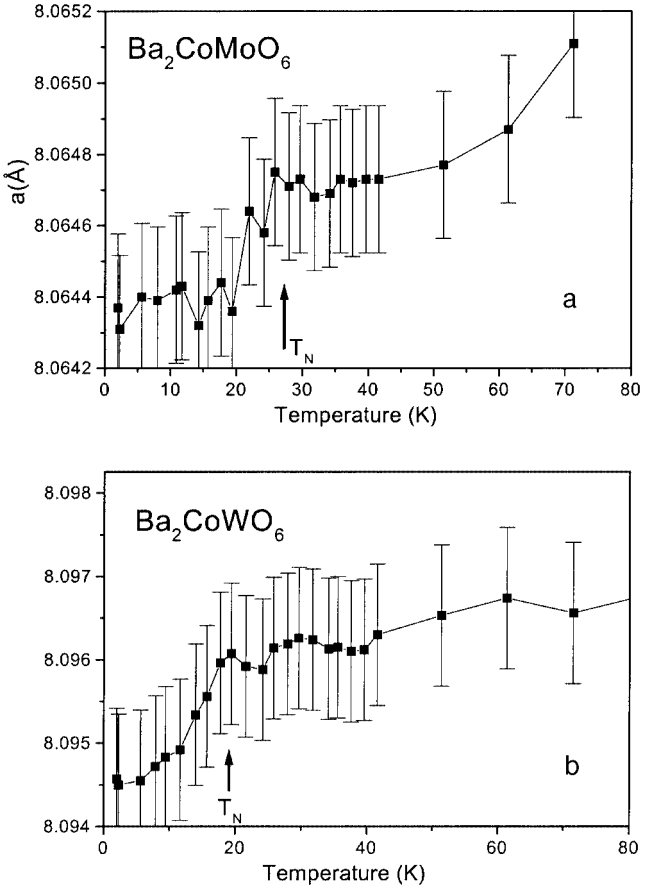

Figure 7. Thermal variation of the a unit-cell parameter for Ba_2CoBO_6: (a) B = Mo (b) B = W

Discussion

Ba_2CoMoO_6 and Ba_2CoWO_6 adopt the well-known $(NH_4)_3FeF_6$ structure, corresponding to a perfect 1:1 B-site ordering, due to the large differences in charge existing between Co^{2+} and $Mo(W)^{6+}$ cations. The refinement of a possible inversion or anti-site disordering confirms an almost complete ordering degree between both cations. A bond valence calculation[21] from the observed bond lengths can give some insight into the actual oxidation states of the different cations present in the crystal structures. In Ba_2CoMoO_6, the calculated valences for Ba, Co and Mo are 2.57, 1.93 and 5.61, respectively; in Ba_2CoWO_6 the calculated valences for Ba, Co and W are 2.51, 1.85 and 5.85, respectively. In both compounds the Ba cations seem to be significantly overbonded, exhibiting valences much higher than the expected 2+ value. In fact, the observed Ba−O distances are much shorter (Table 2) than expected from the sum of the ionic radii (2.95 Å). It seems that the much more covalent network determined by CoO_6 octahedra and BO_6 octahedra (B = Mo, W) mainly determines the size of the unit cell; the low degree of freedom of this cubic crystallographic structure constrains the Ba−O bond lengths outside of the

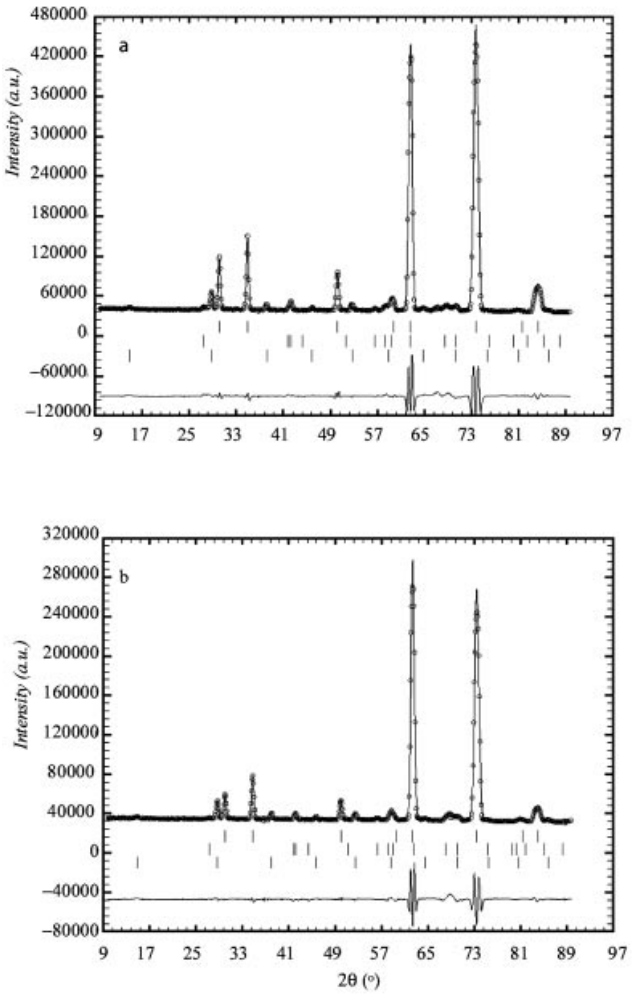

Figure 8. Observed (solid circles), calculated (solid line) and difference (bottom line) NPD patterns collected at 2 K with λ = 2.42 Å; the two series of tick marks correspond to the crystallographic and magnetic Bragg reflections: (a) Ba_2CoMoO_6 (b) Ba_2CoWO_6

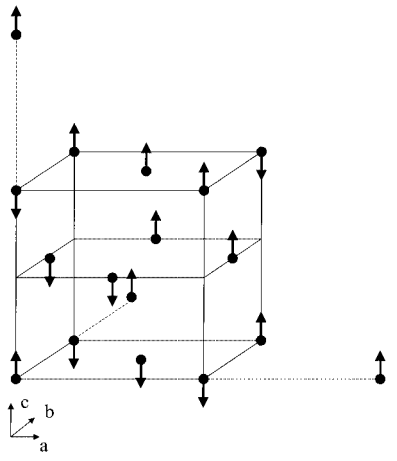

Figure 9. A sketch of the magnetic structure for k = (1/2, 1/2, 1/2); for the sake of clarity, the figure shows the chemical cell ($a \approx 8$ Å) and a part of three adjacent cells

optimal values. This is not an isolated behavior; in many other double perovskites, the Ba−O bond lengths exhibit values within a wide range: for instance, the Ba−O distances range from 2. 85 Å for Ba_2NiWO_6 to 2.96 Å for Ba_2CdWO_6. The valences for Co and Mo(W), although slightly lower than expected, suggest the divalent and hexavalent oxidation states for both cations, respectively.

In relation to the electronic configurations of the B cations, the comparison with Sr_2FeMoO_6 (prepared under reducing conditions and showing half-metallic and ferromagnetic properties) is enlightening: although the actual electronic configurations $Fe^{3+}(3d^5)$-$Mo^{5+}(4d^1)$ vs. $Fe^{2+}(3d^6)$-$Mo^{6+}(4d^0)$ have been considered as possible, the average valence for Fe has been found to be intermediate between high-spin configuration values of Fe^{2+} and Fe^{3+} from Mössbauer spectroscopy studies.[22] The case of $Ba_2Co(Mo,W)O_6$ is rather different: from the chemical point of view, the preparation in air suggests a hexavalent oxidation state for Mo cations, with the Co cations being divalent. From this chemical point of view, the electronic configuration $Co^{2+}(3d^7)$-$Mo(W)^{6+}(4d^0)$ seems to be more probable than $Co^{3+}(3d^6)$-$Mo(W)^{5+}(4d^1)$, although a slight degree of dynamic electron transfer between Co and Mo cations should not be excluded in view of the bond valence results.

To account for the results from the magnetic susceptibility data, the electronic configuration $Co^{2+}(3d^7)$-$Mo^{6+}(4d^0)$ requires a completely unquenched orbital contribution for the high-spin Co^{2+} cation, which would explain the large effective moment obtained in the paramagnetic region, well above T_N, of 5.24 μ_B/f.u. and 5.58 μ_B/f.u for B = Mo, W. Recently, Primo-Martín et al.[23] studied the $Sr_3CoSb_2O_9$ double perovskite, with an effective moment of 5.39 μ_B and also proposed a high-spin Co^{2+} configuration with a completely unquenched orbital contribution ($^4T_{1g}$ term). This is not an isolated observation; many Co^{2+} compounds show effective moments between 3.87 μ_B (spin only) and 5.20 μ_B (spin plus completely unquenched orbital contribution);[24,25] some examples are CoF_2 (μ_{eff} = 5.15 μ_B) or CoO (μ_{eff} = 5.1 μ_B).

In relation to the ordered magnetic moment obtained for Co cations from the refinement of the magnetic structure at 2 K, it seems to saturate at a value close to 2 μ_B, for both compounds with B = Mo, W. Again, this suggests a high spin configuration for the Co^{2+} cations ($t_{2g}^5\ e_g^2$, S = 3/2) as a low-spin configuration would imply S = 1/2. The reduction of the saturation moment with respect to the expected value of 3 μ_B is believed to be due to covalence effects. In fact, the ordered moment is slightly higher for the W compound (Figure 6): this is related to the increase in Co−O atomic distances (as commented above) and a decrease of the orbital overlapping and covalence effects.

Finally, the thermal evolution of the unit cell parameters (Figure 7) seems to indicate a contraction of the unit-cell size at the onset of the antiferromagnetic ordering for both compounds; this effect suggests the possibility of a magneto-elastic coupling, which has not been described before for antiferromagnetic double perovskites. This effect is not common in magnetic oxides, unless the magnetic transition is associated with an electronic fluctuation which is responsible for the change in bonding strength between the metallic element and oxygen; a paradigmatic example is

that of the $RNiO_3$ perovskites,[26] where the AFM transition is coupled with a metal-insulator transition and a dramatic contraction in unit-cell volume is observed upon electron delocalization. The present magneto-volume effect suggests a subtle change in the electron localization concomitant with the AFM transition in the Ba_2CoBO_6 double perovskites.

Conclusions

The study of the crystallographic structure of the double perovskites Ba_2CoMoO_6 and Ba_2CoWO_6 from neutron powder diffraction data allowed us to determine subtle structural features relating the Co−O bond lengths and ordered magnetic moments with the chemical environment in the crystals; the larger electronegativity for W in front of Mo accounts for a more ionic, weaker Co−O bond with a larger magnetic moment for Co in Ba_2CoWO_6. These compounds experience a low-temperature antiferromagnetic ordering characterized by an isotropic propagation vector k = (1/2, 1/2, 1/2), giving rise to antiferromagnetic couplings between each Co moment and the six nearest neighbors. It seems clear that the Co ions adopt a divalent oxidation state, in a high-spin configuration. A completely unquenched orbital contribution for the Co^{2+} cation is necessary to account for the large effective moment obtained in the paramagnetic region A magneto-elastic effect observed at the onset of the antiferromagnetic ordering is unusual in completely localized oxides, suggesting a certain degree of electron itinerancy in these compounds.

Experimental Section

Ba_2CoBO_6 (B = Mo, W) perovskites were prepared as black (B = Mo) or brown (B = W) polycrystalline powders from citrate precursors obtained by soft chemistry procedures. Stoichiometric amounts of analytical grade $Ba(NO_3)_2$, $Co(NO_3)_2{\cdot}6H_2O$, $(NH_4)_6Mo_7O_{24}{\cdot}4H_2O$ or $H_{26}N_6O_{41}W_{12}{\cdot}18H_2O$ were dissolved in citric acid. The citrate + nitrate solutions were slowly evaporated, leading to organic resins containing a random distribution of the involved cations at an atomic level. These resins were first dried at 120 °C and then slowly decomposed at temperatures up to 600 °C. All the organic materials and nitrates were eliminated in a subsequent treatment at 800 °C in air, for 2 hours. This treatment gave rise to highly reactive precursor materials. Afterwards, the resulting black or brown powders were treated at 1100 °C in air for 12 hours.

The initial characterization of the products was carried out by laboratory X-ray diffraction (XRD) (Cu-K_α, λ = 1.5406 Å). Neutron powder diffraction (NPD) diagrams were collected at the Institut Laue-Langevin (ILL) in Grenoble (France). The crystallographic structures were refined from the high resolution NPD patterns, acquired at room temperature at the D2B diffractometer with λ = 1.594 Å. For the determination of the magnetic structures and the study of their thermal variation, a series of NPD patterns were obtained at the D20 high-flux diffractometer (ILL, Grenoble) with a wavelength of 2.42 Å, in the temperature range from 2 to 72 K for B = Mo and 2 to 99 K for B = W. The refinements of both crystal and magnetic structures were performed by the Rietveld method, using the FULLPROF refinement program.[27] A pseudo-Voigt function was chosen to generate the line shape of the diffraction peaks. The coherent scattering lengths for Ba, Co, Mo, W and O were 5.07, 2.49, 6.72, 4.86 and 5.803 fm, respectively. The magnetic form factor considered for the Co^{2+} cation was determined with the coefficients taken from the International Tables of Crystallography. The *dc* magnetic susceptibility was measured with a commercial SQUID magnetometer on powdered samples, in the temperature range 1.5 to 250 K (B = Mo) and 330 K (B = W).

Acknowledgments

We thank the financial support of CICyT to the project MAT2001-0539, and we are grateful to ILL for making all facilities available.

[1] A. P. Ramirez, *J. Phys.: Condens. Matter* **1997**, *9*, 8171.
[2] *Colossal Magnetoresistance and Other Related Properties in 3d Oxides* (Eds.: C. N. R. Rao, B. Raveau), World Scientific: Singapore, **1998**.
[3] K.-I. Kobayashi, T. Kimura, H. Sawada, K. Terakura, Y. Tokura, *Nature* **1998**, *395*, 677.
[4] B. García-Landa, C. Ritter, M. R. Ibarra, J. Blasco, P. A. Algarabel, R. Mahendiran, J. García, *Solid State Commun.* **1999**, *110*, 435.
[5] A. Maignan, B. Raveau, C. Martin, M. Hervieu, *J. Solid State Chem.* **1999**, *144*, 224.
[6] K.-I. Kobayashi, T. Kimura, Y. Tomioka, H. Sawada, K. Terakura, Y. Tokura, *Phys. Rev. B* **1999**, *59*, 11159.
[7] T. H. Kim, M. Uehara, S-W. Cheong, S. Lee, *Appl. Phys. Lett.* **1999**, *74*, 1737.
[8] J. A. Alonso, M. T. Casais, M. J. Martínez-Lope, J. L. Martínez, P. Velasco, A. Muñoz, M. T. Fernández-Díaz, *Chem. Mat.* **2000**, *12*, 161.
[9] C. Ritter, M. R. Ibarra, L. Morellón, J. García, J. M. De Teresa, *J. Phys.: Condens. Matter* **2000**, *12*, 8295.
[10] W. Prellier, W. Smolyaninova, A. Bisbas, C. Galley, R. L. Greene, K. Ramesha, J. Golapakrishnan, *J. Phys.: Condens. Matter* **2000**, *12*, 965.
[11] M. C. Viola, M. J. Martínez-Lope, J. A. Alonso, P. Velasco, J. L. Martínez, J. C. Pedregosa, R. E. Carbonio, M. T. Fernández-Díaz, *Chem. Mat.* **2002**, *14*, 812−818.
[12] F. Galasso, *Structure, Properties and Preparation of Perovskite-Type Compounds*, Pergamon Press, Oxford **1969**.
[13] F. J. Fresia, L. Katz, R. Ward, *J. Am. Chem. Soc.* **1959**, *81*, 4783.
[14] L. J. Brixner, *Phys. Chem.* **1960**, *64*, 165.
[15] Landolt-Bornstein, *Zahlenwerte und Funktionen aus Naturwissenschaften und Technik*, Neue Serie, Band 4, Teil a, Springer-Verlag, Berlin **1970**.
[16] G. Blasse, *Proc. Int. Conf. Mag. Nottingham* 1964, p. 350, Inst. Phys. London **1965**.
[17] A. Bokov, *Soviet Phys.-Solid State (English Trans.)* **1972**, *15*, 400.
[18] B. Khattak, *Mater. Res. Bull.* **1975**, *10*, 1343.
[19] D. E. Cox, G. Shirane, B. C. Frazer, *J. Appl. Phys.* **1967**, *38*, 1459.
[20] R. D. Shannon, *Acta Crystallogr., Sect. A* **1976**, *32,* 751.
[21] N. E. Brese, M. O'Keefe, *Acta Crystallogr., Sect. B* **1991**, *47*, 192.
[22] J. Linden, T. Yamamoto, M. Karppinen, H. Yamauchi, T. Pietari, *Appl. Phys. Lett.* **2000**, *76*, 2925.
[23] V. Primo-Martín, M. Jansen, *J. Solid State Chem.* **2001**, *157*, 76.
[24] R. J. Radwanski, Z. Ropka, *Physica B* **2000**, 281&282, 507.
[25] A. Mahendra, D. C. Khan, *Phys. Rev. B* **1971**, *4*, 3901.
[26] J. L. García-Muñoz, J. Rodríguez-Carvajal, P. Lacorre, J. B. Torrance, *Phys. Rev. B* **1992**, *46*, 4414.
[27] J. Rodríguez-Carvajal, *Physica B* (Amsterdam) **1993**, *192*, 55.

Received January 29, 2002
[I02047]